Delft University of Technology

Implementation of Fully Coupled Electromigration Theory in COMSOL

Cui, Zhen; Fan, Xuejun; Zhang, Kouchi

DOI
10.1109/ECTC51906.2022.00046

Publication date
2022

Document Version
Final published version

Published in
Proceedings of the 2022 IEEE 72nd Electronic Components and Technology Conference (ECTC)

Citation (APA)
Cui, Z., Fan, X., & Zhang, K. (2022). Implementation of Fully Coupled Electromigration Theory in COMSOL. In L. O'Conner (Ed.), *Proceedings of the 2022 IEEE 72nd Electronic Components and Technology Conference (ECTC)* (pp. 233-238). Article 9816390 IEEE. https://doi.org/10.1109/ECTC51906.2022.00046

Important note
To cite this publication, please use the final published version (if applicable).
Please check the document version above.

Copyright
Other than for strictly personal use, it is not permitted to download, forward or distribute the text or part of it, without the consent of the author(s) and/or copyright holder(s), unless the work is under an open content license such as Creative Commons.

Takedown policy
Please contact us and provide details if you believe this document breaches copyrights.
We will remove access to the work immediately and investigate your claim.

This work is downloaded from Delft University of Technology.
For technical reasons the number of authors shown on this cover page is limited to a maximum of 10.

Green Open Access added to TU Delft Institutional Repository

'You share, we take care!' - Taverne project

https://www.openaccess.nl/en/you-share-we-take-care

Otherwise as indicated in the copyright section: the publisher
is the copyright holder of this work and the author uses the
Dutch legislation to make this work public.

Implementation of Fully Coupled Electromigration Theory in COMSOL

Zhen Cui[2], Xuejun Fan[1,2], Guoqi Zhang[2]
[1]Department of Mechanical Engineering, Lamar University, Beaumont, TX 77710, USA
[2]Department of Microelectronics, Delft University of Technology, Delft, 2628 CD, Netherlands
xuejun.fan@lamar.edu

2022 IEEE 72nd Electronic Components and Technology Conference (ECTC) | 978-1-6654-7943-1/22/$31.00 ©2022 IEEE | DOI: 10.1109/ECTC51906.2022.00046

***Abstract*— In this paper, a 3D and fully coupled electromigration modeling is implemented using COMSOL. The fully coupled multi-physics theory has a unique set of partial differential equations, which cannot be directly simulated with the standard finite element software such as ABAQUS and ANSYS. With the weak form PDE modulus in COMSOL, the weak form of the governing equations is obtained and realized for a 3D finite element modeling of electromigration. The metal lines under totally constrained and stress-free conditions with a perfectly blocking condition are presented as benchmark problems, in which the finite element solutions are in excellent agreement with the analytical solutions.**

Keywords-electromigration; general coupling theory; multi-physics modeling; finite element analysis.

I. Introduction

Electromigration is an enhanced mass transport process in metal interconnects induced by high electrical current density, which, over time, causes void nucleation near the cathode side and hillock development near the anode side, resulting in opens and shorts in microelectronic devices [1-5]. The driving force of electromigration is attributed to the momentum transfer between conducting electrons and diffusion metal atoms, which is vividly called the electron wind force. However, the intense electric currents in interconnects during electromigration are accompanied by the gradients of atomic concentration, mechanical stress, and temperature [6-10]. These gradients become the driving forces of mass transport coupled with electron wind force.

With the continued scaling down of interconnect technology, electromigration remains one of the critical reliability issues in the integrated circuit and packaged device. As such, it has been a focus of intense experimental study and numerical simulation [11]. Based on the accurate numerical modeling method, the prediction of time-to-failure (TTF) of interconnects under high current density can complement experiments to optimize the interconnect structure and improve its reliability [12-15]. Over the past decades, there are many research works on the formulation and solution of electromigration. Korhonen *et al*. [16] developed a widely used model that couples the stress evolution with vacancy transport. Then, Rzepka *et al*. [17] implement Korhonen's model in ANSYS for finite element analysis. Sarychev *et al*. [18] proposed an even more general physical model to evaluate the stress development during electromigration, in which a sophisticated constitutive model was established. Then, Lin and Basaran implemented this model in ABAQUS and conducted the FE modeling of electromigration in pure metal line and solder joint [19-21]. Furthermore, Sukharev *et al*. [22, 23] also developed a multi-physics model and implemented it in a general commercial FE software. However, some of the coupling terms in those electromigration models are inconsistent and incomplete in one way or another as discussed in refer. [6] and [7].

Recently, a general coupling model (GCM) for electromigration has been developed, in which all physical fields and their effects on electromigration are considered and fully coupled [6]. And. The GCM has been implemented in ANSYS published in refer. [24-28]. In the GCM model, the diffusion equation (mass conservation equation) is not a standard form of the diffusion equation in the built-in multi-physics theory in ANSYS. Therefore, the effective diffusivity concept has been derived and introduced, and consequently, the diffusion equation is reduced to a standard diffusion equation without the source/sink term. Additionally, the diffusion strain equation must be linearized in order to use the standard form of ANSYS built-in equation.

COMSOL Multiphysics provides strong solvers and user-friendly interfaces to find the solutions to any form of PDEs using weak form modeling. Users only need to input weak-form expressions for the PDEs required to be solved. In this paper, based on the fully coupled theory with a new diffusion strain equation we developed recently [7], the weak forms of governing equations are obtained, and the 3D finite element modeling of electromigration is achieved. The detailed description and implementation procedure using COMSOL are presented. The conductor under fully-constrained and stress-free configurations with perfectly blocking boundary conditions are used as benchmark problems to verify the implementation.

II. Fully-Coupled Theory of Electromigration

Based on the general coupling model presented in the paper [6] and diffusion-induced strain developed in paper [29] (*Microelectronics Reliability* 120, 114127, 2021), a fully-coupled theory of electromigration is proposed. Here, we briefly introduce the key equations. Mass conservation equation is used to describe the EM (see Eq. (1)), in which θ is the total volumetric strain and $\boldsymbol{J}_a$ is the total atomic flux which is a combination of the fluxes caused by the gradients

2377-5726/22/$31.00 ©2022 IEEE
DOI 10.1109/ECTC51906.2022.00046

Authorized licensed use limited to: TU Delft Library. Downloaded on January 26,2023 at 09:43:36 UTC from IEEE Xplore. Restrictions apply.

of concentration, electrical potential, mechanical stress, and temperature,

$$\frac{\partial \theta}{\partial t} = -\Omega \nabla \cdot \boldsymbol{J}_a \tag{1}$$

$$\boldsymbol{J}_a = D_a(-\nabla C_a - C_a \frac{Z^* e \rho j}{k_B T} + C_a \frac{\Omega \nabla \sigma}{k_B T} - C_a \frac{Q^* \nabla T}{k_B T^2}) \tag{2}$$

where D_a is the atomic diffusivity, j is the current density, e is the elementary charge, ρ is the electrical resistance, Z^* is the effective charge number ($Z^* > 0$), σ is the hydrostatic stress, and Q^* is the heat of atomic transport.

The total volumetric strain θ in Eq. (1) is a sum of the elastic strain $\boldsymbol{\varepsilon}^{me}$, the thermal strain $\boldsymbol{\varepsilon}^{th}$, and the diffusion-induced strain $\boldsymbol{\varepsilon}^{diff}$,

$$\theta = \mathrm{tr}(\boldsymbol{\varepsilon}) \tag{3}$$

$$\boldsymbol{\varepsilon} = \boldsymbol{\varepsilon}^{me} + \boldsymbol{\varepsilon}^{th} + \boldsymbol{\varepsilon}^{diff} \tag{4}$$

$$\boldsymbol{\varepsilon}^{th} = \alpha (T - T_0) \boldsymbol{I} \tag{5}$$

$$\varepsilon^{diff} = \int_{C_{a0}}^{C_a} \frac{1-f}{3} \frac{dC_a}{C_a} \boldsymbol{I} \tag{6}$$

where α is the coefficient of thermal expansion and $\boldsymbol{I}$ is the unit tensor. T_0 is the initial temperature, and f is the vacancy relaxation factor.

Considering that the material is linearly elastic and isotropic, the stress-strain relation can be described based on the Hooke's law as follows:

$$\boldsymbol{\sigma} = 2G\boldsymbol{\varepsilon} + \lambda tr(\boldsymbol{\varepsilon})\boldsymbol{I} - Btr(\boldsymbol{\varepsilon}^{th})\boldsymbol{I} - Btr(\boldsymbol{\varepsilon}^{diff})\boldsymbol{I} \tag{7}$$

$$\sigma = tr(\boldsymbol{\sigma})/3 \tag{8}$$

where G and λ are Lamé constants, $2G=E/(1+\upsilon)$ and $\lambda = 2G\upsilon/(1-2\upsilon)$, E is the Young's modulus, υ is the Poisson's ratio, $B = \lambda + 2G/3$ is the bulk modulus.

As the vacancy transport equation is coupled with stress, electrical, and temperature fields, thus above equations must be solved together with the governing equations of stress, displacement, strain, electric field, and temperature. These equations are given as follows:

$$\nabla \cdot \boldsymbol{\sigma} + \boldsymbol{F} = 0 \tag{9}$$

$$\boldsymbol{\varepsilon} = \frac{1}{2}(\nabla \boldsymbol{u} + \boldsymbol{u}\nabla) \tag{10}$$

$$\nabla \cdot \boldsymbol{j} = 0 \tag{11}$$

$$\boldsymbol{j} = \frac{\boldsymbol{E}}{\rho} = -\frac{\nabla V}{\rho} \tag{12}$$

$$k\nabla^2 T + \boldsymbol{j} \cdot \boldsymbol{E} = 0 \tag{13}$$

where $\boldsymbol{F}$ is the body force, $\boldsymbol{u}$ is the displacement vector, $\boldsymbol{E}$ is the electric field, and k is the thermal conductivity.

III. Finite Element Implementation

An overview of implementation procedures is illustrated in Fig. 1. There are three key steps, global definition, variation definition, and weak forms of governing equations, which are introduced in detail below. Through those three steps, Eqs. (1) – (13) can be completed implemented in COMSOL without any approximation. According to the specific problems, we create geometry models, set initial and boundary conditions, and adapt meshing strategy to do the FE analysis.

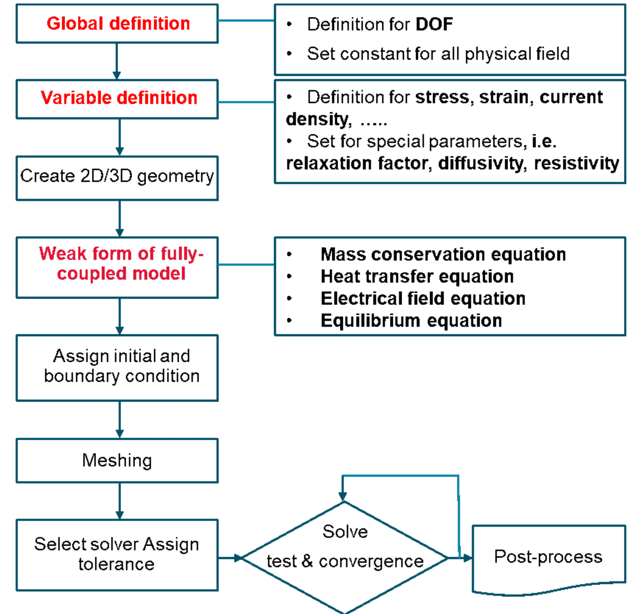

Figure 1. overview of implementation procedure in COMSOL

A. DOFs and Global definition

First, we need to define the degree of freedoms for FE analysis based on the fully-coupled theory.

- Define C for the concentration;
- T for the temperature;
- ψ for the electric potential;
- u, v, and w for the displacements in x, y, and z, respectively.
- Moreover, some constants used in Eqs. (1)-(13) are set, such as Boltzmann constant (k_B) and elementary charge (e).

B. Variable definition

Variables used in the governing equations for each physical field need to be defined.

Authorized licensed use limited to: TU Delft Library. Downloaded on January 26,2023 at 09:43:36 UTC from IEEE Xplore. Restrictions apply.

- For the electrical field, we need to define the electric field and current density according to Eq. (12), and the electron wind force.
- For the thermal field, we define the source of heat as $j^2\rho$, and temperature gradient (∇T).
- For strains, we need to define the total strain based on Eq. (10), and the thermal strain and diffusion strain are written in COMSOL based on Eqs. (5) and (6), respectively. Then, the elastic strain is defined as total strain minus diffusion strain and thermal strain.
- Mechanical stress components are defined based on the Hooke's laws and hydrostatic stress shown in Eqs. (7) and (8) need to be defined.

C. Weak form of fully-coupled theory

Following Eqs. (14) – (19) are the weak forms for the mass conservation equation (1), the equilibrium equation (9), the electric field equation (11), and the heat transfer equation (13).

$$\int_\Phi t(C)\frac{\partial\theta}{\partial t}dV+\int_\Phi \Omega(\frac{\partial t(C)}{\partial x}J_{ax}+\frac{\partial t(C)}{\partial y}J_{ay}+\frac{\partial t(C)}{\partial z}J_{az})dV \\ -\int_{\partial\Phi}\Omega t(C)(J_{ax}+J_{ay}+J_{az})d\Gamma=0 \tag{14}$$

$$\int_\Phi \begin{matrix}[\frac{\partial t(u)}{\partial x}(C_{1111}\frac{\partial u}{\partial x}+C_{1122}\frac{\partial v}{\partial y}+C_{1133}\frac{\partial w}{\partial z}) \\ \frac{\partial t(u)}{\partial y}C_{1212}(\frac{\partial u}{\partial y}+\frac{\partial v}{\partial x})+\frac{\partial t(u)}{\partial z}C_{1313}(\frac{\partial w}{\partial x}+\frac{\partial u}{\partial z})]\mathrm{dV}\end{matrix} \\ +\int_\Phi t(u)f_x dV-\int_{\partial\Phi}t_x t(u)d\Gamma=0 \tag{15}$$

$$\int_\Phi \begin{matrix}[\frac{\partial t(u)}{\partial x}(C_{1111}\frac{\partial u}{\partial x}+C_{1122}\frac{\partial v}{\partial y}+C_{1133}\frac{\partial w}{\partial z}) \\ \frac{\partial t(u)}{\partial y}C_{1212}(\frac{\partial u}{\partial y}+\frac{\partial v}{\partial x})+\frac{\partial t(u)}{\partial z}C_{1313}(\frac{\partial w}{\partial x}+\frac{\partial u}{\partial z})]\mathrm{dV}\end{matrix} \\ +\int_\Phi t(u)f_x dV-\int_{\partial\Phi}t_x t(u)d\Gamma=0 \tag{16}$$

$$\int_\Phi \begin{matrix}[\frac{\partial t(u)}{\partial x}(C_{1111}\frac{\partial u}{\partial x}+C_{1122}\frac{\partial v}{\partial y}+C_{1133}\frac{\partial w}{\partial z}) \\ \frac{\partial t(u)}{\partial y}C_{1212}(\frac{\partial u}{\partial y}+\frac{\partial v}{\partial x})+\frac{\partial t(u)}{\partial z}C_{1313}(\frac{\partial w}{\partial x}+\frac{\partial u}{\partial z})]\mathrm{dV}\end{matrix} \\ +\int_\Phi t(u)f_x dV-\int_{\partial\Phi}t_x t(u)d\Gamma=0 \tag{17}$$

$$\int_\Phi t(T)\ j^2\rho dV+\int_\Phi k(\frac{\partial t(T)}{\partial x}\frac{\partial T}{\partial x}+\frac{\partial t(T)}{\partial y}\frac{\partial T}{\partial y}+\frac{\partial t(T)}{\partial z}\frac{\partial T}{\partial z})dV \\ +\int_{\partial\Phi}kt(T)(\frac{\partial T}{\partial x}+\frac{\partial T}{\partial y}+\frac{\partial T}{\partial z})d\Gamma=0 \tag{18}$$

$$\int_\Phi \frac{1}{\rho}(\frac{\partial t(V)}{\partial x}\frac{\partial V}{\partial x}+\frac{\partial t(V)}{\partial y}\frac{\partial V}{\partial y}+\frac{\partial t(V)}{\partial z}\frac{\partial V}{\partial z})dV \\ +\int_{\partial\Phi}t(T)\frac{1}{\rho}(\frac{\partial V}{\partial x}+\frac{\partial V}{\partial y}+\frac{\partial V}{\partial z})d\Gamma=0 \tag{19}$$

IV. Benchmark Problems

A. Totally Confined aluminum line

A 1-D totally confined aluminum line with perfectly blocking condition is studied as a benchmark problem, as shown in Fig.2 (a). For the sake of simplicity, the Joule heating effect is ignored in this study, thus no temperature gradient for the entire model. Table I shows the material properties of metal line. The mesh of conductor is shown in Fig. 2(b).

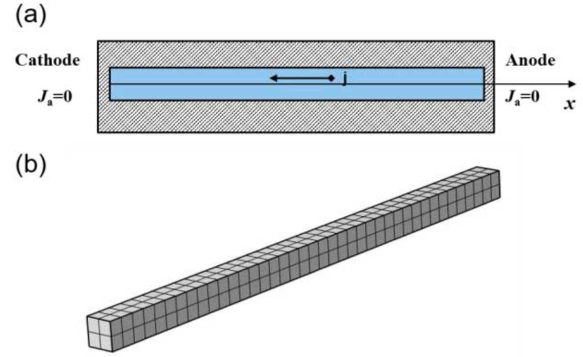

Figure 2. (a) Al line embedded in a rigid passivation layer. (b) mesh of conductor used in FEA simulation.

Following initial and boundary conditions are implied:

- Initial condition: $C_a(x)=C_{a0}$ and $T=475\mathrm{K}$.
- Diffusion boundary condition: the vacancy flux is blocked at both sides of metal line, $J_a(0) = J_a(L) = 0$.
- Mechanical boundary condition: metal line is embedded in a rigid passivation layer, $v = w = 0$ and $u(0) = u(L) = 0$.

TABLE I. MATERIAL PROPERTIES

Length of the metal line (L)	200 μm
Young's modulus (E)	70 GPa
Poisson ratio (v)	0.3
Atomic diffusivity (D_a)	1×10^{-14} m²/s
Atomic volume (Ω)	1.66×10^{-29} m³
Electrical resistivity (ρ)	4.88×10^{-8} Ohm·m
Current density (j)	1.0×10^{10} A/m²
Elementary charge (e)	1.6×10^{-19} C
Charge number (Z*)	1.1
Boltzmann constant (k_B)	1.38×10^{-23} J/K

Authorized licensed use limited to: TU Delft Library. Downloaded on January 26,2023 at 09:43:36 UTC from IEEE Xplore. Restrictions apply.

Vacancy relaxation factor (f)	0.7

To verify the FE results, the analytical solution of this 1-D problem shown in paper [7] is used to compare with the FEA results.

Fig. 3(a) plots the normalized atomic concentration along the length of Al line, in which atoms accumulate at the cathode side and decrease at the anode side. This indicates that atoms transport along the opposite direction of the current density. Fig. 3(b) shows the tensile stress at the cathode side due to the depletion of atoms, and the compressive stress at the anode side. At 1000 s, 2000 s, and the steady state, the FEA results are in excellent agreement with the numerical results obtained from analytical solutions.

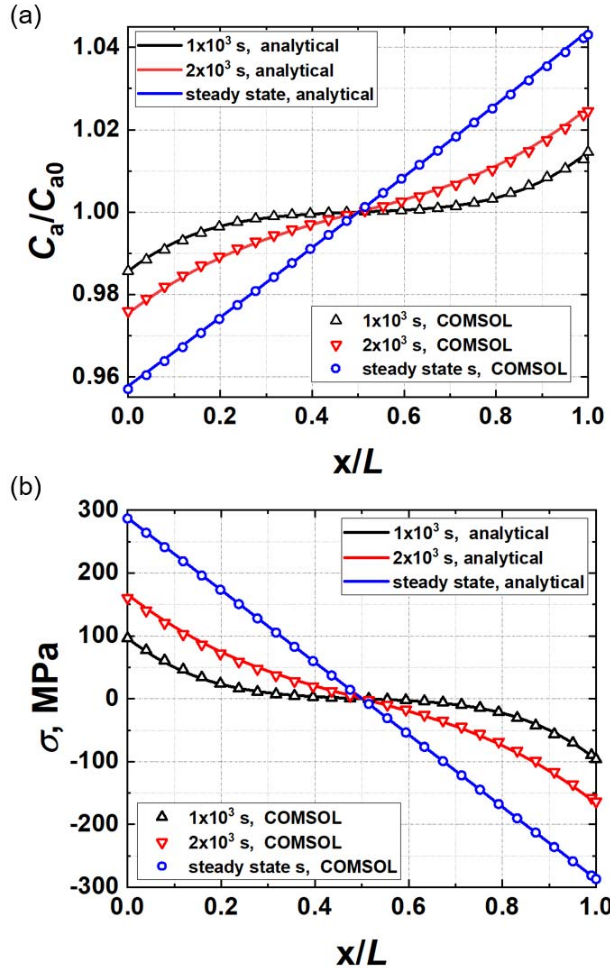

Figure 3. (a) Distribution of atomic concentration along the length of conductor in totally constrained condition. (b) Distribution of hydrostatic stress along the length of conductor in totally constrained condition.

B. Stress-free aluminum line

A 1-D stress-free Al line with perfectly blocking condition is studied, as shown in Fig. 4. Following initial and boundary conditions are implied:

- Initial condition: $C_a(x) = C_{a0}$ and $T = 475\text{K}$.
- Diffusion boundary condition: the vacancy flux is blocked at both sides of metal line, $J_a(0) = J_a(L) = 0$.
- Mechanical constrains are applied as shown in Fig. 4(b) to remove the rigid displacement.

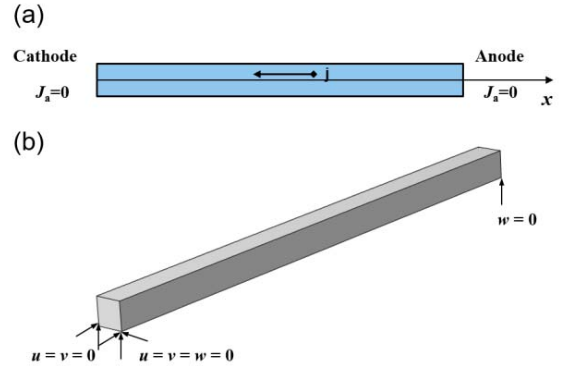

Figure 4. (a) Schematic for a stress-free Al line. (b) Applied constrains for conductor in FEA simulation.

Fig. 5 plots the normalized atomic concentration distributed along the Al line. At 5000 s, 2×10^4 s, and 10^5 s, the FEA results from COMSOL are nearly identical to the analytical solution. Fig. 6 plots the evolution of atomic concentration at the cathode side over time. The FEA results are in excellent agreement with analytical solutions at transient state. Fig. 6 also shows that the decrease of atomic concentration in stress-free conductor is much faster than that in fully-constrained conductor. The EM in fully-constrained conductor can reach the steady state at ~6 h, but the EM in stress-free conductor still develops at ~14 h. This differences indicate that the stress gradient plays an important role in reducing EM.

Authorized licensed use limited to: TU Delft Library. Downloaded on January 26,2023 at 09:43:36 UTC from IEEE Xplore. Restrictions apply.

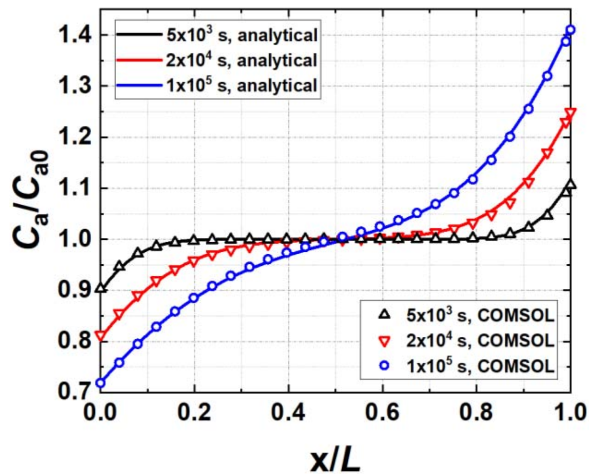

Figure 5. Distribution of normalized atomic concentration along the length of stress-free metal line.

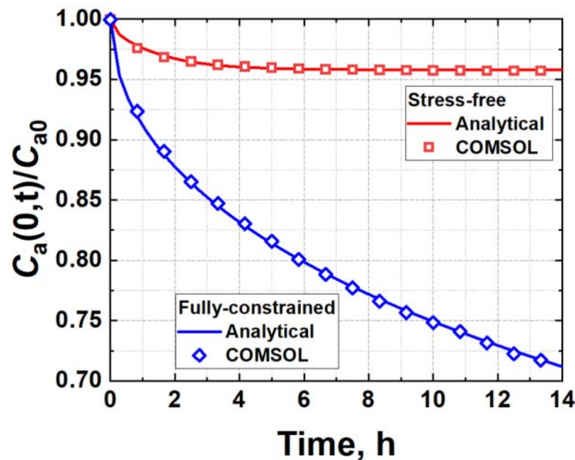

Figure 6. Evolution of normalized atomic concentration over time at x=0 for totally constrained and stress-free conductors.

CONCLUSION

In this paper, a newly developed fully-coupled model for electromigration is implemented in COMSOL using the weak form PDE mode. Weak forms for governing equations of the fully-couped theory were obtained. The implementation procedure in COMSOL was presented. As a validation, the obtained 1-D FE solutions for conductors under fully-constrained and stress-free configurations are in excellent agreement with the analytical solutions at both transient and steady states.

REFERENCES

1. Tan, C.M. and A. Roy, *Electromigration in ULSI interconnects.* Materials Science and Engineering: R: Reports, 2007. **58**(1-2): p. 1-75.
2. Ho, P.S. and T. Kwok, *Electromigration in metals.* Reports on Progress in Physics, 1989. **52**(3): p. 301.
3. Tu, K.-N., Y. Liu, and M. Li, *Effect of Joule heating and current crowding on electromigration in mobile technology.* Applied Physics Reviews, 2017. **4**(1): p. 011101.
4. Fan, X., *New Results on Electromigration Modeling in Microelectronics*. 2019: Electronic Packaging Society (EPS) Webinar.
5. Zhang, Y., et al., *The effect of atomic density gradient in electromigration.* International Journal of Materials Structural Integrity, 2012. **6**(1): p. 36-53.
6. Cui, Z., X. Fan, and G. Zhang, *General coupling model for electromigration and one-dimensional numerical solutions.* Journal of Applied Physics, 2019. **125**(10): p. 105101.
7. Cui, Z., *MULTI-PHYSICS DRIVEN ELECTROMIGRATION STUDY: MULTI-SCALE MODELLING AND EXPERIMENT.* Delft University of Technology, 2021. **Doctor dissertation**.
8. Kirchheim, R. and U. Kaeber, *Atomistic and computer modeling of metallization failure of integrated circuits by electromigration.* Journal of applied physics, 1991. **70**(1): p. 172-181.
9. Cui, Z., et al., *Effects of Temperature and Grain Size on Diffusivity of Aluminium: Electromigration Experiment and Molecular Dynamic Simulation.* Journal of Physics: Condensed Matter, 2022.
10. Dandu P., *Finite Element Modeling of Electromigration in Wafer Level Packages*. 2012, Ph.D. Dissertation, Lamar University.
11. Fan, X., B. Varia, and Q. Han, *Design and optimization of thermo-mechanical reliability in wafer level packaging.* Microelectronics Reliability, 2010. **50**(4): p. 536-546.
12. Dandu, P., et al., *Finite element modeling on electromigration of solder joints in wafer level packages.* Microelectronics Reliability, 2010. **50**(4): p. 547-555.
13. Ma, R., et al. *Electromigration simulation of flip chip CSP LED*. in *2017 18th International Conference on Electronic Packaging Technology (ICEPT)*. 2017. IEEE.
14. Taner, O., K. Kijkanjanapaiboon, and X. Fan. *Does current crowding induce vacancy concentration singularity in electromigration?* in *2014 IEEE 64th Electronic Components and Technology Conference (ECTC)*. 2014. IEEE.
15. Dandu, P. and X. Fan. *Assessment of current density singularity in electromigration of solder bumps*. in *2011 IEEE 61st Electronic Components and Technology Conference (ECTC)*. 2011. IEEE.
16. Korhonen, M., et al., *Stress evolution due to electromigration in confined metal lines.* Journal of Applied Physics, 1993. **73**(8): p. 3790-3799.
17. Rzepka, S., et al. *3-D finite element simulator for migration effects due to various driving forces in interconnect lines*. in *AIP Conference proceedings*. 1999. American Institute of Physics.
18. Sarychev, M., et al., *General model for mechanical stress evolution during electromigration.* Journal of Applied Physics, 1999. **86**(6): p. 3068-3075.
19. Lin, M. and C. Basaran, *Electromigration induced stress analysis using fully coupled mechanical–diffusion equations with nonlinear material properties.* Computational Materials Science, 2005. **34**(1): p. 82-98.
20. Basaran, C. and M. Lin, *Damage mechanics of electromigration induced failure.* Mechanics of Materials, 2008. **40**(1-2): p. 66-79.
21. Yao, W. and C. Basaran, *Computational damage mechanics of electromigration and thermomigration.* Journal of Applied Physics, 2013. **114**(10): p. 103708.
22. Sukharev, V. and E. Zschech, *A model for electromigration-induced degradation mechanisms in dual-inlaid copper interconnects: Effect of interface bonding strength.* Journal of Applied Physics, 2004. **96**(11): p. 6337-6343.
23. Sukharev, V., E. Zschech, and W.D. Nix, *A model for electromigration-induced degradation mechanisms in dual-inlaid copper interconnects: Effect of microstructure.* Journal of Applied Physics, 2007. **102**(5): p. 053505.

Authorized licensed use limited to: TU Delft Library. Downloaded on January 26,2023 at 09:43:36 UTC from IEEE Xplore. Restrictions apply.

24. Cui, Z., X. Fan, and G. Zhang. *Implementation of General Coupling Model of Electromigration in ANSYS*. in *2020 IEEE 70th Electronic Components and Technology Conference (ECTC)*. 2020. IEEE.

25 Dandu P, Fan XJ, Liu Y. Some remarks on finite element modeling of electromigration in solder joints. Proc of 60th Electronic Components and Technology Conference (60th ECTC), Las Vegas, NV, USA, 396-402, 2010.

26 Fan XJ, Liu Y. Design, reliability and electromigration in chip scale wafer level packaging. Electronic Components and Technology Conference (59th ECTC), Professional Development Course Notes. June, 2009.

27. Kijkanjanapaiboon K., Modeling of Electromigration and Lock-in Thermography in Micro-electronics Packaging. Doctoral Dissertation, Lamar University. 2017.

28. Taner O, Investigation of the Effect of Current Singularity on Vacancy Concentration in 2D Coupled Electromigration. Master Thesis, Lamar University. May 2014..

29. Cui, Z., X. Fan, and G. Zhang, *Molecular dynamic study for concentration-dependent volume relaxation of vacancy.* Microelectronics Reliability, 2021. **120**: p. 114127.

Authorized licensed use limited to: TU Delft Library. Downloaded on January 26,2023 at 09:43:36 UTC from IEEE Xplore. Restrictions apply.